Applied Composite Materials
https://doi.org/10.1007/s10443-020-09836-0

Curing Cycle Optimization for Thick Composite Laminates Using the Multi-Physics Coupling Model

Zhenyi Yuan[1] · Xinxing Tong[1] · Guigeng Yang[1] · Zhenchao Yang[1] · Danlong Song[1] · Shujuan Li[1] · Yan Li[1]

Received: 26 July 2020 / Accepted: 16 October 2020

Abstract
A multi-objective optimization method which takes the multi-physics coupling characteristic into account is proposed to determine the cure cycle profile for polymer-matrix composites. First, a numerical model which considers the effects of heat transfer, cure kinetics, resin flow-compaction process has been developed to predict the temperature and degree of curing. The simulation results agree well with the experimental measurements from the previous publication to validate the practicability of the FE model. A surrogate model based on the Surface Response Method is built to make the solution feasible according to the entire calculation time. The surrogate model was integrated into the optimization framework to optimize cure cycle profile using NSGA-II algorithm. The results show that the duration of the cure time and the maximum gradient of temperature are about 44.8% and 34% shorter than in the typical cure profile, respectively. It is also shown that the multi-physics coupling characteristic should be considered in the optimization process for thick composite component.

Keywords Polymer-matrix composites (PMCs) · Cure behaviour · Numerical analysis · Cure

1 Introduction

During the past decades, the use of polymer-matrix composite materials (PMCs) in advanced engineering applications such as aerospace, automobile, and sport technologies has expanded widely due to the their good mechanical properties and weight savings than those of other conventional materials. There are lots of methods to produce composite components, such as autoclave process [1], resin transfer molding process [2], hot diaphragm forming [3] and vacuum film infusion [4]. Up till the present moment, autoclave curing process has been widely used in the manufacturing of high-performance PMCs components. In the autoclave cure process of composite, the component is subjected to

✉ Zhenyi Yuan
yuanzhenyi2007cs@163.com

[1] School of Mechanical and Instrument Engineering, Xi'an University of Technology, Xi′an 710048, Shaanxi, China

a temperature–pressure-time profile known as cure cycle. In the beginning, the viscosity of resin becomes sufficiently low with the increase of curing temperature. Then the autoclave applied pressure squeezes the excess resin and air bubbles out of the laminate. With the temperature continually rising to elevated value, the PMCs sustains irreversible cross-linking reaction and cures into a rigid component. However, the exothermic reaction of resin during the cross-linking process and the low thermal conductivity of material usually result in severe temperature peak and uneven distribution of temperature for thick laminate, resulting in matrix cracks, residual stress and possibly degradation of the composite [5–7]. Meanwhile, the autoclave process of PMCs generally needs high equipment costs and long processing time [8]. Therefore, the optimization of the cure process for thick composite laminate is necessary to increase the production rates, reduce the likelihood of process defects and minimize the manufacturing costs of composite components.

Generally the cure cycle profile recommended by the material manufacturers is relevant to thin laminate. For thick laminate, the selection of cure cycle profile is usually based on a trial-and-error method or the experience of technologists and these methods are very timing wasting. Using low curing temperature may reduce or eliminate the process defects, the cure time will inevitably increase to guarantee the fully cured of composite component. On the contrary, cure time will be shortened using high curing temperature, the process-induced defects could occur in such a situation. How to find the appropriate cure profile in presence of minimizing temperature gradient and minimizing cure time simultaneously is a multi-objective optimization problem. In fact, optimization problems exist widely and vary in the real world. Unlike simple optimization problems, multi-objective optimization problems (MOP) have several objectives that need to be optimized, and these objectives conflict with each other [9]. The multi-objective optimization methods have been widely used in structural or process parameters optimum design [10–12].

In earlier optimization research of cure process, minimizing the cure time has always been investigated as single objective. The temperature overshoot or temperature gradient has been incorporated as constraints in these optimization models [13–15]. In other investigations, the weighted combination of several optimization sub-objectives has been developed to determine the optimal cure profile. However, the selection of weight coefficient is relatively important for the optimization process under different objectives and these methods have limited exploration considering the multi-dimensional objective space [13–16]. The optimization problem of cure process requires simultaneous consideration of the different objectives related to product quality and manufacturing cost. Therefore, multi-objective optimization methods are used to overcome this limitation by treating the two objectives independently to reach trade-off between quality and cost. These approaches, based on the combination of computer FE model for cure process and numerical optimization strategy, have been widely used in the multi-objective optimization of PMCs [17–19]. The cure process is usually simulated as a non-isothermal problem, using some commercial software such as ANSYS, ABAQUS and MSC.Marc.

It is should be noted that multi-objective optimization for cure process demands hundreds of FE analysis. Thus, cure process optimization using the FE model is computationally expensive and becomes too large to handle with computing resources. An alternative is to employ a surrogate model to overcome this issue. In the surrogate model, the relationship between design variables and output responses, such as temperature and cure time is established using mathematical model [20]. Aleksendrić et al. [19, 21] proposed a computational procedure which is based on the coupling of dynamic artificial neural model and genetic algorithms to achieve pre-series optimization of cure cycle profile for PMCs. Tifkitsis et al. [22] proposed a multi-objective optimization method based on Kriging

method substituting the FE model to reduce the computation effort required for the optimization process. As we can see, the above optimization methods combined with cure process simulation model or surrogate model have been widely used to determine the cure cycle profile for composite material. In these optimization methods, better understanding the cure process of composite is the basis, and the effectiveness of the cure process FE model or surrogate model is very important. However, the cure process of composite has a multi-physics coupling characteristic. Such research is beneficial and detailed, but fails to involve the effects of resin viscosity and resin flow-compaction process. The temperature distribution obtained during cure process of composite is not only influenced by the applied curing temperature profile, but also the applied pressure in autoclave. Gutowski et al. [23] conducted consolidation experiments and proposed the SSM model (squeezed sponge model), in which the effective stress theory is utilized to calculate the flow-compaction of composites during the cure process. In the SSM model, the autoclave pressure is shared by the resin and fiber, and the fiber bed will undertakes more pressure with the resin flowing out. Young [24, 25] extended SSM by considering multidirectional fiber arrangements and predicted flow velocity of the resin and laminate thickness of the composite laminates during the cure process. Li et al. [26] and Ganapathi et al. [27] study the effect of bleeder on the consolidation of the laminate and found that the temperature distribution depends heavily on the resin flow-compaction process in thick laminate.

As of now, there is little study in the previous optimization method which accounts for the multi-physics coupling characteristic of cure process. These methods which not consider the resin flow-compaction process may lead to an inexact forecasting of temperature and DoC distribution for thick laminate. As a result, it is essential to develop an optimization method that accounts for all the physical phenomena during curing process of composite. This paper presents a framework for the analysis and optimization of cure cycle profile for thick composite laminate by taking the phenomena such as heat transfer, cure kinetics, and resin flow-compaction process into consideration in a composite manufacturing process. The optimization in the framework consists of a multi-physics coupling model and an optimization method. The paper is organized as follows: The curing multi-physics coupling model of composite in the autoclave process is described in Sect. 2. Based on the cure process model, a sampling method has been employed to generate combinations of the design variables of the cure process and then a surrogate model based on the Response Surface Methodology is built in Sect. 3. The calculated results obtained from the surrogate model are compared with the FEM result to validate the accuracy. Then an optimization method is used to optimize the cure cycle profile of thick composite laminate. In Sect. 4, the comparison result of the optimization method with and without multi-physics coupling characteristic is described. The summary and conclusions of this work are drawn in Sect. 5.

2 Multi-Physics Coupling Model for Cure Process of Composite

As mentioned above, three critical phenomena are included in the autoclave process: (a) the heat transfer with a volumetric generation term indicating the exothermic chemical reaction, (b) the viscosity variation of resin, (c) resin flow associated with compaction behavior.

2.1 Thermo-Chemical Model

The developments of temperature and DoC inside the composite laminate are calculated using the thermo-chemical model. This model combines the heat conduction with resin chemical reaction. In this model, the key point is to take the nonlinear heat source due to the resin curing reaction into consideration. Governing equation for heat transfer analysis derived from energy conservation and Fourier's law can be expressed in Eq. (1) [28]:

$$\frac{\partial}{x}\left(\lambda_x \frac{\partial T}{\partial x}\right) + \frac{\partial}{y}\left(\lambda_y \frac{\partial T}{\partial y}\right) + \frac{\partial}{z}\left(\lambda_z \frac{\partial T}{\partial z}\right) + Q = \rho_c C_c \frac{\partial T}{\partial t} \tag{1}$$

where λ_i $(i=x, y, z)$ is thermal conductivity of the composite; ρ_c is the density of composite; C_c is the specific heat capacity of the composite; T is the transient temperature, t is the cure time. The subscript c and r refer to composite and resin material, respectively. The interior heat source Q is bound up with the cure kinetics and can be expressed as follows:

$$Q = \rho_r(1 - V_f)H_r \frac{\mathrm{d}\alpha}{\mathrm{d}t} \tag{2}$$

where the subscript f refer to fiber material. V_f is the fiber volume fraction of the composite; α is the DoC of the resin;H_r is the total release heat by resin exothermic chemical reaction. As we can see, the heat source Q is related to the fiber volume fraction V_f of the composite. The fiber volume fraction V_f can be updated using the consolidation model in Sect. 2.3. As we know, the resin itself generates lots of heat due to complex chemical reactions in the cure process. These heat releases are related to the cure rate da/dt. In this study, the cure kinetics model for 3501–6 epoxy resin can be expressed as follows [28, 29]:

$$\frac{\mathrm{d}\alpha}{\mathrm{d}t} = \begin{cases} (K_1 + K_2\alpha)(1-\alpha)(0.47-\alpha) & (\alpha \le 0.3) \\ K_3(1-\alpha) & (\alpha > 0.3) \end{cases} \tag{3}$$

In which

$$K_i = A_i \exp\left(\frac{-\Delta E_i}{RT}\right) \quad (i = 1, 2, 3) \tag{4}$$

In which R is a universal gas constant; A_i is the frequency factor and ΔE_i is the activation energy[30].

The density and specific heat capacity of the composite are calculated using the following mixture in Eq. (5) and Eq. (6) [30], respectively. For 3501–6 resin, the specific heat capacity is related to temperature and DoC, as shown in Eq. (7) [31].

$$\rho_c = V_f\rho_f + (1 - V_f)\rho_r \tag{5}$$

$$C_c = \frac{V_f\rho_f C_f + (1 - V_f)\rho_r C_r}{\rho_c} \tag{6}$$

$$C_r = 4184 \times \left(0.468 + 5.975 \times 10^{-4}T - 0.141\alpha\right) \tag{7}$$

The fiber conductivity is assumed to be transversely isotropic, while the resin conductivity λ_r is isotropic, as shown in Eq. (8). The thermal conductivity of composite is also calculated making use of the mixture rules [32, 33], as shown in Eq. (9) and Eq. (10).

As we can see, the thermal conductivity of composite relies on the fiber volume fraction, which can be updated in the resin flow-compaction model.

$$\lambda_r = 0.04184 \times [3.85 + (0.035T - 0.141)] \tag{8}$$

$$\lambda_1 = \lambda_r(1 - V_f) + \lambda_f^{\mathrm{L}} V_f \tag{9}$$

$$\frac{\lambda_2}{\lambda_r} = \frac{\lambda_f^{\mathrm{T}} + \lambda_r + \left(\lambda_f^{\mathrm{T}} - \lambda_r\right)V_f}{\lambda_f^{\mathrm{T}} + \lambda_r - \left(\lambda_f^{\mathrm{T}} - \lambda_r\right)V_f} \tag{10}$$

where λ_f^{L}andλ_f^{T} are the thermal conductivity of the fiber in the longitudinal and transverse direction, respectively. The properties of 3501–6 epoxy resin and AS4 fiber can be found in Table 1.

2.2 Resin Viscosity Model

The viscosity of resin during consolidation relies on the rheological behavior of the composite system. In this study, the 3501–6 resin is used and this resin viscosity model can be expressed using the process temperature and DoC, as shown in [34].

$$\eta = \eta_\infty \exp\left(\frac{U}{RT} + \eta_\beta \alpha\right) \tag{11}$$

where η_∞ is the reference viscosity constant; U is the activation energy; η_β is a constant which is independent of curing temperature.

2.3 Resin Flow-Compaction Model

The composite laminate is consolidated by the curing pressure which is applied for a specific time. As the viscosity of resin decreases and the autoclave pressure is applied, the excess resin will flow out of the laminate, which results in a decrease of laminate thickness. With the assumption the applied pressure is shared by the resin and fiber at any location of the laminate, the force equilibrium equation at any instant of the cure process can be described as follows [35]:

Table 1 Properties of 3501–6 epoxy resin and AS4 fiber

Symbol	Value	Source
ρ_r/kg·m^{-3}	90 α + 1 232 ($\alpha \leq 0.45$) 1 272 ($\alpha > 0.45$)	[31]
ρ_f/kg·m^{-3}	1790	[34]
C_f/J·(kg·K)$^{-1}$	750 + 2.05 × T(℃)	[30]
λ_f^{L}/W·(m·K)$^{-1}$	7.69 + 0.0156 × T(℃)	[30]
λ_f^{T}/W·(m·K)$^{-1}$	2.4 + 0.00507 × T(℃)	[30]

$$P = P_{\mathrm{f}} + P_{\mathrm{r}} \tag{12}$$

where P is total externally pressure in the autoclave; P_{f} is the fiber effective stress and P_{r} is the hydraulic pressure of resin. The resin flow-compaction model can be expressed as follows using the Darcy Law and effective compaction stress [36]:

$$\frac{1}{\eta m_{\mathrm{v}}}\left[k_x\frac{\partial^2 P_{\mathrm{r}}}{\partial x^2} + k_y\frac{\partial^2 P_{\mathrm{r}}}{\partial y^2} + k_z\frac{\partial^2 P_{\mathrm{r}}}{\partial z^2}\right] = \frac{\partial P_{\mathrm{r}}}{\partial t} \tag{13}$$

where k is the permeability of the composite which is anisotropic; m_{v} is the coefficient of volume compressibility that can be expressed as [37]:

$$m_{\mathrm{v}} = -\frac{\mathrm{d}e}{\mathrm{d}P_{\mathrm{f}}}\frac{1}{(1+e)} \tag{14}$$

where e is the void ratio of composite $e = \left(1/V_f\right) - 1$ and it can be described as a relationship with fiber effective stress [31]:

$$e = \begin{cases} -1.555\,2\times10^{-6}P_{\mathrm{f}} + 1.476 & \left(P_{\mathrm{f}} \le 68.7\ \mathrm{kPa}\right) \\ -0.491\ \log_{10}P_{\mathrm{f}} + 3.745 & \left(P_{\mathrm{f}} > 68.7\ \mathrm{kPa}\right) \end{cases} \tag{15}$$

The fiber permeability can be expressed using the following equation:

$$k_1 = \frac{r_f^2\left(1-V_f\right)^3}{(2.8V_f)^2} \tag{16}$$

$$k_2 = k_3 = \frac{r_f^2\left[\left(0.8/V_f\right)^{0.5} - 1\right]^3}{\left[0.8\left(0.8/V_f\right) + 1\right]} \tag{17}$$

where r_{f} is the fiber radius. The properties of resin and fiber are reported in Table 1 and Table 2, respectively. After the cure process, the final laminate thickness h can be calculated using the following equations [31]:

Table 2 Properties for the cure kinetics of 3501–6 epoxy resin

Symbol	Value	Source
H_{r} /J·kg^{-1}	473 600	[34]
R /J·(mol·K)$^{-1}$	8.3143	-
η_∞/Pa·s	7.93×10^{-14}	[34]
U /J·mol^{-1}	9.08×10^{4}	
η_β	14.1	
A_1 /min^{-1}	2.101×10^{9}	
A_2 /min^{-1}	-2.014×10^{9}	
A_3 /min^{-1}	1.96×10^{5}	
ΔE_1 /J·mol^{-1}	8.07×10^{4}	
ΔE_2 /J·mol^{-1}	7.78×10^{4}	
ΔE_3 /J·mol^{-1}	5.66×10^{4}	

$$h = \left(\frac{1+e}{1+e_0}\right)h_0 \tag{18}$$

where e_0 and h_0 are the initial void ratio and thickness of the laminate, respectively.

2.4 Numerical Validation Verification

The accuracy of the numerical model was confirmed by comparing the simulation result of multi-physical coupling FE model with experimental result measured by Shin and Han [31]. A 228-ply AS4/3501–6 laminate with initial fiber volume fraction 40.383% was fabricated in Ref. [31]. The initial temperature and DoC are set as 26 ℃ and 0.0001, respectively. Then the temperature increases to 121.1 ℃ at a temperature rising rate 2.22 ℃/min. Then at the first holding-stage, the temperature is kept at 121.1 ℃ for 60 min. After the first holding-stage, the laminate is heated at 2.22 ℃/min to the second holding-stage. After that, the laminate is cured at 176.7 ℃ for 120 min. At last, the temperature drops to 26 ℃ at 2.22 ℃/min, as shown in Fig. 1. The dimension of the laminate is 152.6×152.6×35.76 mm. The silicon rubber was placed at the perimeter of the laminate to prevent excess resin flowing out from the side. Eighteen bleeder plies were placed on top of the laminate to absorb the resin that flows out from the laminate. Therefore, it was one-dimensional flow through the thickness and an adiabatic condition can be maintained at these sides. The non-porous peel ply between the mould and the prepreg stack is so thin enough that it does not affect the heat transfer significantly and may be ignored. There are no bleeder plies on the mould side, therefore impermeable flow condition is defined for the bottom surface of the laminates. The top surface of laminate is subjected to forced air convection boundary condition, while ambient temperature same as cure profile is applied on the bottom boundary to simplify the cure simulation model. A 2D finite element (FE) model of the cross section

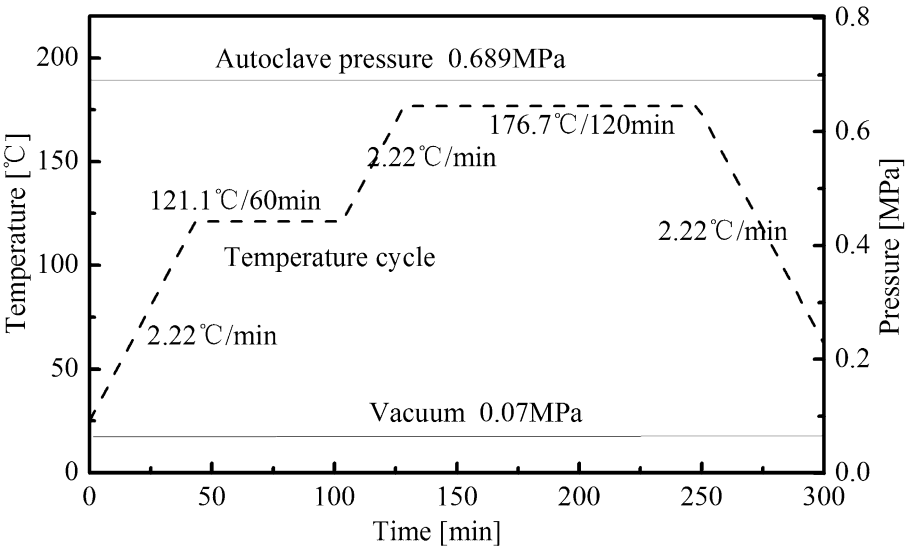

Fig. 1 Curing cycle profile of AS4/3501–6 prepregs

is developed to simulate the cure process of the thick laminate. Due to the symmetric of the cross section and boundary conditions, only half of the section is modeled using 400 elements with dimensions of 76.3×35.76 mm, as shown in Fig. 2. Antonucci et al. [38] found that the heat transfer coefficient H in autoclave can range from 30 to 100 W/(m^2·K) and the influence of the heat transfer coefficient is relatively small compared to the effect of laminate thickness. In this work, the sensitivity analysis by changing the coefficient is also conducted, as shown in Fig. 3. As we can see, the effect of heat transfer coefficient on the maximum curing temperature is not obvious. Hence, the surface heat transfer coefficient of the top surface in the multi-physics coupling model is set to 38 W/(m·K) to represent

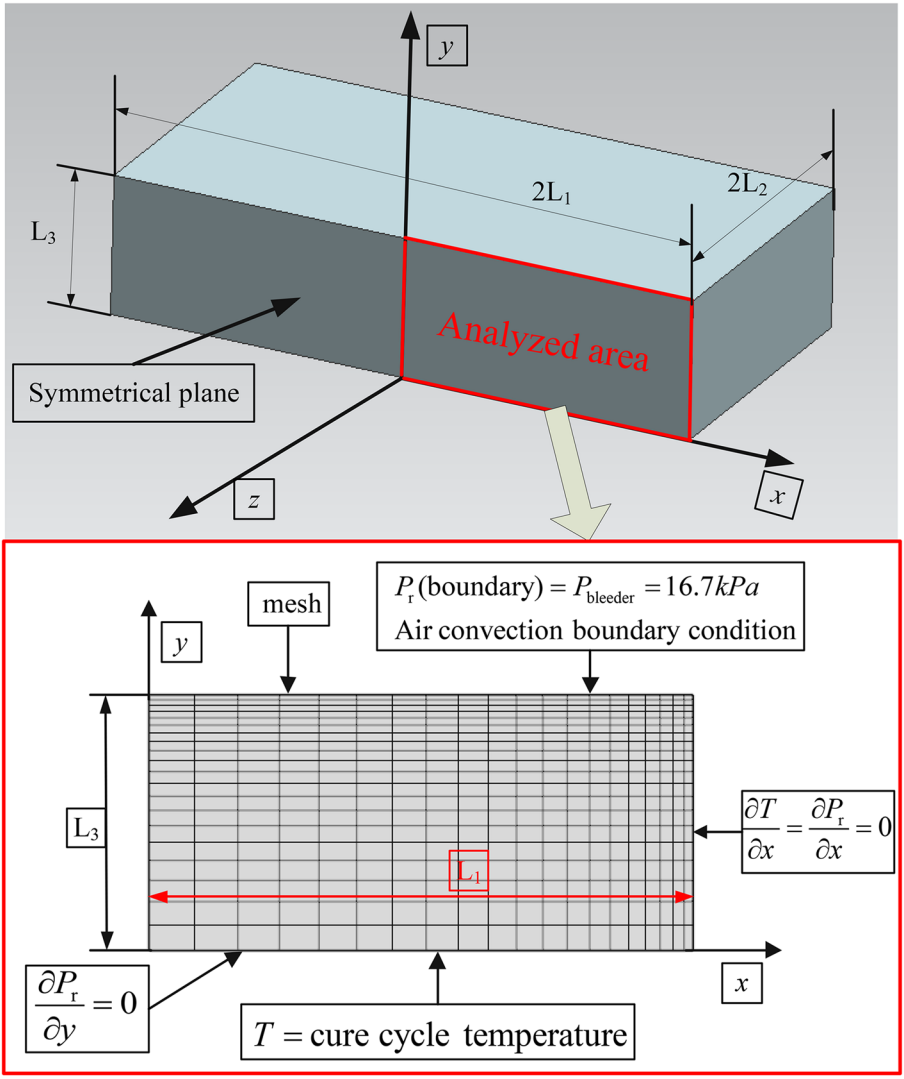

Fig. 2 Schematic of finite element model boundary conditions

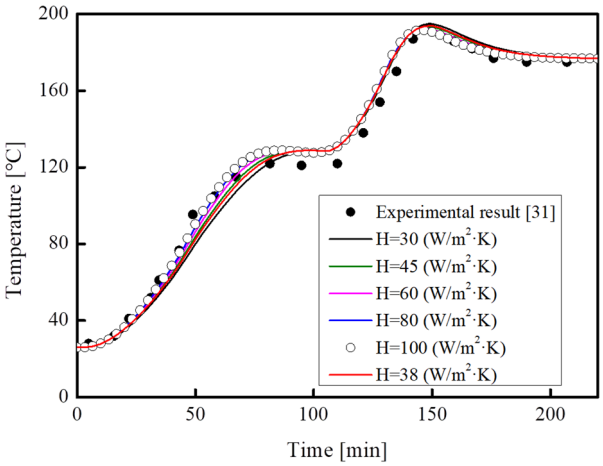

Fig. 3 The effect of heat transfer coefficient H on the development of temperature

the conditions in the autoclave, which is same as the boundary condition employed in the literature [28]. The simulation time increment is 20 s, which is appropriate to demonstrate the multi-physical coupling characteristic of the FE model with good efficiency. The practical curing time was 5.02 h, while the simulation CPU time is 10 min on a PC.

Figure 4 shows the temperature history at central point of the laminate, which is compared to the experimental results. The calculated results of thickness reduction are also compared in Fig. 5. As we can see, the laminate thickness decreased from 35.76 mm to

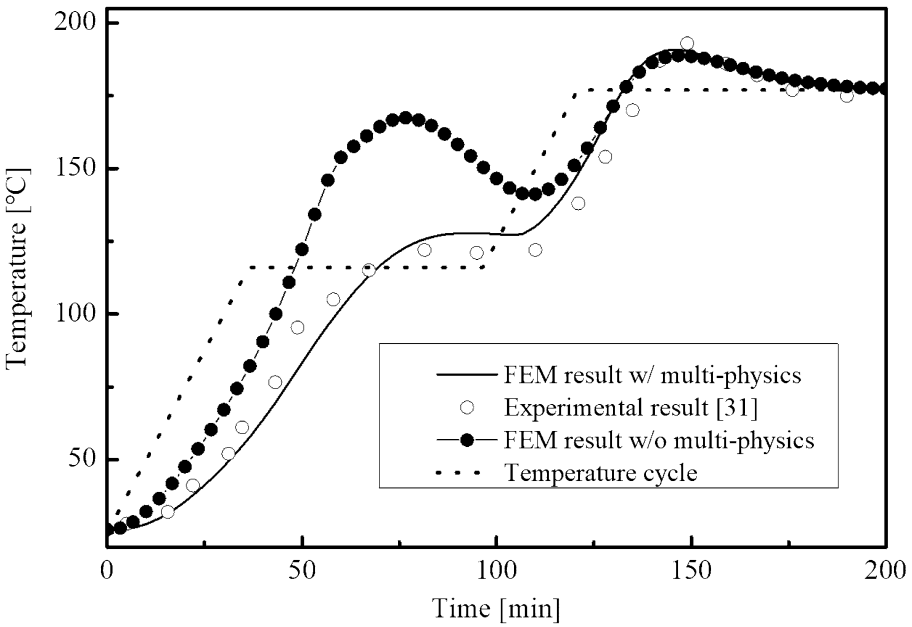

Fig. 4 Simulation results and experimental results of temperature with the cure cycle profile

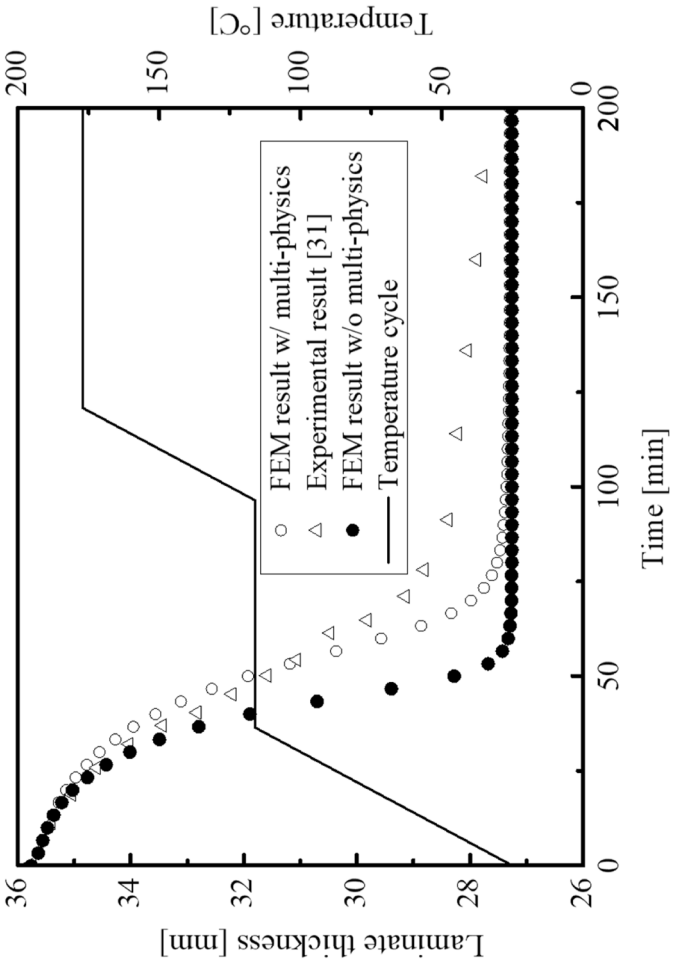

Fig. 5 Simulation results and experimental results of laminate thickness with the cure temperature cycle

27.26 mm and the maximum temperature gradient during the cure process reaches 17.4 ℃. The comparison results of temperature and thickness history validate the accuracy of the multi-physics coupling model established in this paper. Figure 4 also shows the development of temperature at the center of the laminate with and without the resin flow-compaction process into consideration. A clear distinction in the temperature profile can be seen at the first heating- and holding-stage. The development of resin viscosity and DoC using the two different models is shown in Fig. 6. As we can see, the curves of DoC are directly related to the temperature profile in Fig. 4 due to the temperature dependency of the DoC. From 0 to 120 min, higher temperature calculated using the FE model w/o multi-physics leads to higher cure kinetics reaction. Thus, the viscosity of resin in the model w/o multi-physics decreases faster than the case in the multi-physics model. This is the reason why the decrease rate of laminate thickness in the multi-physics model was slower than that in the model w/o multi-physics model, as shown in Fig. 5. At the low viscosity, the resin will outflow from the laminate as result of the applied autoclave pressure, which leads to a decrease of resin content in the laminate. Subsequently, the contribution of exothermic reaction of resin will decrease when compared to the results without resin flow-compaction process into consideration. Therefore, a multi-physics coupling FE model is more appropriate to capture the temperature development during cure process for thick composite laminate.

3 Multi-Objective Optimization of the Cure Cycle Profile for Thick Laminate

In this section, a multi-objective optimization method is proposed based on the developed multi-physics coupling FE model and multi-objective optimization algorithm NSGA-II. The stability and efficiency of the algorithm NSGA-II has been proved for the multi-objective curing optimization of composite materials [39]. In order to optimize the cure cycle, the

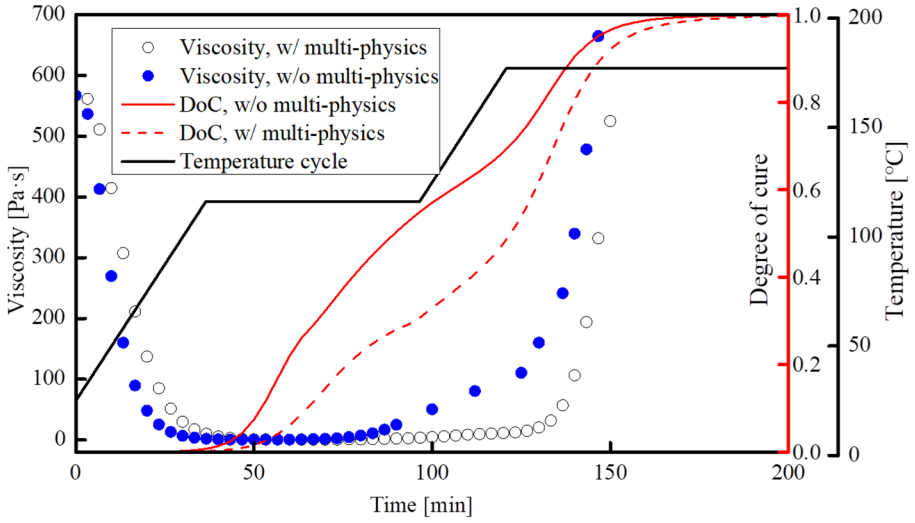

Fig. 6 Simulation results of resin viscosity and DoC using different mode

optimization goal should be identified first. Esposito et al. [40] discussed the influence of temperature overshoot on the mechanical behavior of composite part. The interlaminar shear strength decreases with the increase of temperature overshoot. Meanwhile, curing residual stresses may result from thermal gradients through the thickness of the part after gel point (AGP). After AGP, the resin transforms from liquid state to solid state and begins to transfer the mechanical stress. For the present material system used in this work, the residual stress starts with an initial DoC equal to 0.5 [41]. Thus, the maximum temperature gradient should be minimized after DoC equal to 0.5. For the autoclave process, minimizing the cure time is tantamount to reduce manufacturing cost. Thus, another objective of the optimization in this work is to minimize the cure time. Considering the computing resources becomes too large when the multi-objective optimization algorithm NSGA-II and multi-physics coupling FE model are combined. Therefore, a surrogate model is developed to overcome this problem. Actually, the surrogate technique has been already used for modeling and optimization purposes for cure process of composite [11, 20, 22]. Among the various kinds of surrogate models, the Response Surface Methodology (RSM) model has been proved as a good choice for approximating deterministic computer models [11, 20, 22]. Using the RSM method, the interaction effects between the variables on the responses can be obtained through a small number of samples [42]. In this work, the Response Surface Methodology was used to develop the surrogate model. What's more, the effective transverse modulus is severely influenced by the DoC [20]. The value of the effective transverse modulus is reduced by less than 3% for DoC = 0.96. Therefore, the minimum DoC α_{min} is set 0.96 to satisfy the effective transverse modulus of the lamina and make sure that the composite parts are fully cured. It should be noted that the degradation of matrix is also occurred at higher curing temperature. Therefore, the maximum curing temperature is another constraint. The following are the steps of the multi-objective optimization process.

Step 1: The multi-objectives of this optimization are minimizing the maximum temperature gradient ΔT_{max} and the cure time t_{cycle} simultaneously. In the cure cycle profile, there are six design variables that can be optimized, namely, the first and second holding-stage temperature CT_1 and CT_2, the first and second holding-stage time t_1 and t_2, the first and second temperature rising rate r_1 and r_2. Thus, the optimization can be written mathematically in Eq. (19) The design space of each variable is listed in Table 3. The optimization problem is now defined in the following equation:

$$\begin{aligned} &\text{Find} \quad X=\left(CT_1, CT_2, t_1, t_2, r_1, r_2\right) \\ &\text{Min} \quad t_{cycle}, \quad \Delta T_{max} \\ &S.T. \quad a_{min} \geq 0.96, \quad T_{max} \leq 220^{\circ} \end{aligned} \tag{19}$$

Table 3 The design space of each variable

Symbol	Maximum Value	Minimum Value
CT_1 /℃	100	150
CT_2 /℃	155	220
r_1 /(℃/min)	0.5	3
r_2/(℃/min)	0.5	3
t_1/min	30	120
t_2/min	30	120

Step 2: We generate random samples which is the combination of the six variables using the Latin Hypercube Sampling technique in MATLAB. Compared to the Monte Carlo technique, the samples generated by LHS technique presents better distribution in the entire scope. In the LHS technique, the numbers of samples is independent of the number of input variables. These samples generated by LHS technique were then input into the multi-physics coupling FE model to derive the response T_{max}, t_{cycle}, ΔT_{max} and α_{min}. With these random samples and corresponding outputs, a response surface method (RSM) with cubic polynomial equation form was used to establish the surrogate model, as shown in Eq. (20). The $\mathbf{X}$ represents the input variable vector (CT_1, CT_2, r_1, r_2, t_1, t_2). The Y_i represents the output variable vector (T_{max},t_{cycle},ΔT_{max},α_{min}).

$$\begin{aligned} Y_i(\mathbf{X}) &= \beta_0 + \beta_1 X_1 + \beta_2 X_2 + \cdots + \beta_M X_M + \beta_{M+1} X_1^2 + \beta_{M+2} X_2^2 + \cdots \\ &+ \beta_{2M} X_M^2 + \beta_{2M+1} X_1^3 + \beta_{2M+2} X_2^3 + \cdots + \beta_{3M} X_M^3 + \sum\nolimits_{i \neq j} \beta_{ij} X_i X_j \end{aligned} \tag{20}$$

Step 3: The NSGA-II algorithm included in MATLAB is applied to solve the optimization problem using the surrogate model.

4 Results and Discussion

Before starting the cure optimization for the laminate in Ref [31]. using the present method, we randomly generate another 10 new samples using the LHS technique in order to validate the accuracy surrogate model. It should be noted that $(N+1)(N+2)/2+N$ training samples are required for the construction of the third order RSM model, where N is the number of design variables [42]. Therefore, the minimum required number of training samples is 34 with 6 design variables in this study. In order to obtain more accurate model, 140 training samples are used to build the RSM model. The comparison results of maximum temperature gradient ΔT_{max}, maximum curing temperature T_{max}, minimum DoC α_{min} and cure time t_{cycle} are shown in Table 4. As we can see, the maximum difference between the FEM results and surrogate model results is 11.74%, proving the good efficiency of the surrogate model. The validation of the surrogate model was also conducted using four different error type methods, including relative average absolute error (RAAE), relative maximum absolute error (RMAE), root mean square error (RMSE), and determination coefficient (R^2) [43], as shown in Eq. (21) to Eq. (24). Once the four error values achieve the acceptance levels, the accuracy of the RSM model can be also verified and the RSM model can be used in optimization simulation. As shown in Table 5, all the four error analysis values of the RSM model are at acceptable level, proving the accuracy and robustness of the input–output relationship model.

$$\mathrm{RAAE} = \frac{\sum_{i=1}^{p} \left| Y(x_i) - \hat{Y}(x_i) \right|}{p\sigma} \tag{21}$$

$$\mathrm{RMAE} = \frac{\max\limits_{1 \le i \le p} \left| Y(x_i) - \hat{Y}(x_i) \right|}{\sigma} \tag{22}$$

Table 4 The comparison of FEM results and surrogate model results

Variables						FEM results				Surrogate model results				Relative error			
CT_1	CT_2	r_1	r_2	t_1	t_2	a_{min}	T_{max}	ΔT_{max}	t_{cycle}	a_{min}	T_{max}	ΔT_{max}	t_{cycle}	a_{min}	T_{max}	ΔT_{max}	t_{cycle}
120.60	192.11	2.97	2.68	92.06	89.52	1.00	203.63	21.90	240.17	0.999	202.96	21.57	235.08	0.06%	0.33%	1.48%	2.12%
116.31	207.88	1.59	2.78	119.94	51.03	1.00	214.09	26.36	260.59	0.990	216.98	28.75	246.13	1.03%	-1.35%	-9.08%	5.55%
126.66	168.66	2.31	1.36	107.33	39.56	0.95	172.41	14.11	221.32	0.953	174.44	13.72	221.64	-0.27%	-1.18%	2.75%	-0.15%
106.03	214.02	0.93	1.62	56.02	35.62	1.00	218.12	17.62	244.18	0.992	219.77	16.04	249.23	0.76%	-0.76%	8.99%	-2.07%
135.97	180.84	1.52	2.54	112.05	44.18	0.984	181.19	19.65	246.31	0.983	184.18	20.17	247.12	0.08%	-1.65%	-2.67%	-0.33%
148.1	181.15	0.61	1.92	71.86	74.26	0.998	182.38	17.57	362.6	1.000	182.52	18.45	350.04	-0.25%	-0.08%	-5.03%	3.46%
112.52	206.49	0.96	1.33	51.72	52.66	1.00	209.91	11.16	265.15	0.995	210.50	9.85	270.73	0.46%	-0.28%	11.74%	-2.10%
116.42	155.66	0.96	2.54	60.82	71.34	0.900	173.11	17.45	241.92	0.915	173.25	18.52	249.91	-1.71%	-0.08%	-6.16%	-3.30%
137.2	219.8	2.74	1.49	94.85	55.57	1.00	220.47	19.4	246.33	1.008	220.29	19.03	249.71	-0.75%	0.08%	1.92%	-1.37%
120.41	179.02	1.82	2.83	50.99	62.88	0.988	200.39	23.94	186.5	0.981	198.02	23.27	184.46	0.66%	1.18%	2.82%	1.09%

Table 5 Error analysis results of surrogate models

Error type	T_{max}	ΔT_{max}	t_{cycle}	a_{min}	Acceptance level
RAAE	0.028	0.063	0.033	0.058	<0.2
RMAE	0.062	0.1571	0.082	0.154	<0.2
RMSE	0.036	0.075	0.041	0.073	<0.2
R^2	0.990	0.927	0.971	0.944	>0.9

$$\mathrm{RMSE} = \sqrt{\frac{\sum_{i=1}^{p}\left(Y(x_i) - \hat{Y}(x_i)\right)^2}{p}} \tag{23}$$

$$\mathrm{R}^2 = 1 - \frac{\sum_{i=1}^{p}\left[Y(x_i) - \hat{Y}(x_i)\right]^2}{\sum_{i=1}^{p}\left[Y(x_i) - \overline{Y}(x_i)\right]^2} \tag{24}$$

where p is the number of test points; $Y(x_i)$ is the i-th tested value obtained by FE model; $\hat{Y}(x_i)$ is the predicted value from surrogate model in the i-th test point; $\overline{Y}(x_i)$ is the mean value of the test point; σ is the standard deviation of actual values of validation points.

The computational time is obviously shortened by using the surrogate model. The surrogate model takes only 0.1 min to perform one time computation, whilst the FE model needs 2 min on a Hexa Core CPU (3.2 GHz) PC. Henceforth, this surrogate model derived from the 140 samples simulation was used in the NSGA-II algorithm included in MATLAB to solve the multi-objective optimization problem. The population size is 100 and the number of generations is 50. The total design cure profiles generated for the optimization process are 5000 to derive the optimal Pareto Front. The optimal Pareto front of the multi-objective optimization is shown in Fig. 7. As we can see, if the maximum temperature gradient is prioritized, the long cure time will be difficult to avoid. When the cure time is shorten, the maximum temperature gradient will increase during cure process. Therefore, there is a competition among the ΔT_{max} and the t_{cycle}.

For the sake of fully understanding the effect of the design variables on the objectives, the correlation table of the design variables on objectives is shown in Fig. 8. It is very easy to understand the relationship between and maximum temperature gradient ΔT_{max} and holding-stage temperature CT_2 or holding-stage time t_1. As mentioned above, resin chemical reaction could happen during cure process and temperature at the middle area in the laminate will become significantly more than the surface temperature. Once the second holding-stage temperature CT_2 increases, the temperature on the bottom or top surface of the laminate will increase and the maximum temperature gradient ΔT_{max} between the middle and bottom or top area of the laminate will decrease. Similarly, if longer holding-stage time t_1 is used as cure parameter, higher CT_2 is needed at the second holding-stage to make sure the composite fully cured in a short period time, and thus the ΔT_{max} will also decrease. Therefore, the holding-stage temperature CT_2 or holding-stage time t_1 has negative effect on the temperature gradient ΔT_{max}. On the contrary, the first holding-stage temperature CT_1 and heating rate r_2 has positive effects on the ΔT_{max}. If lower CT_1 or lower r_2 are used

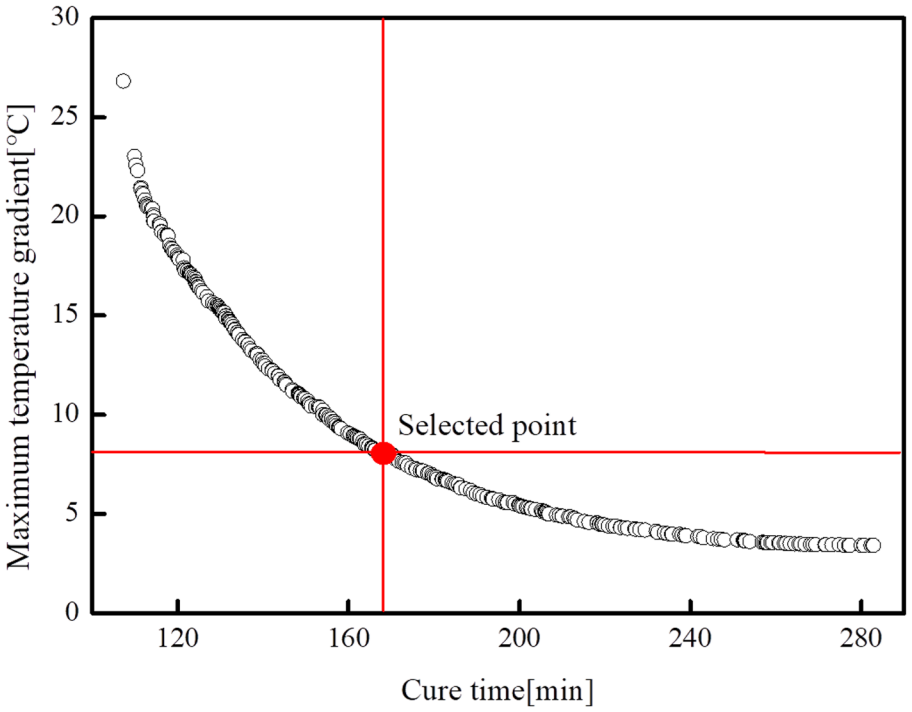

Fig. 7 The Pareto front of the optimization result

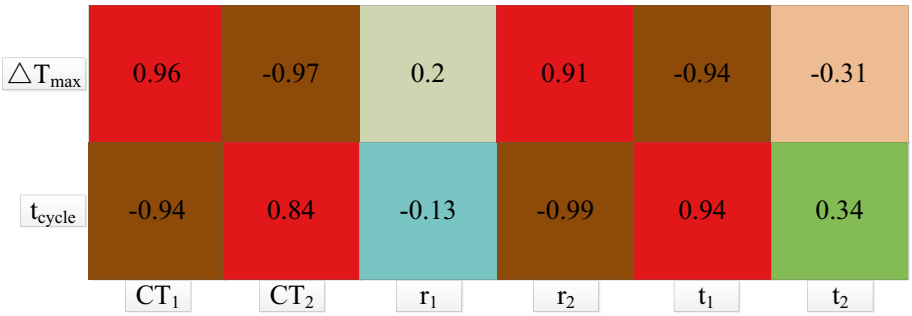

Fig. 8 The correlation table of the variables and objectives

as cure parameters and other cure parameters keep constant, higher CT_2 should be applied in order to fully cure the laminate in a relatively short period of time, which will lead to the decreasing of ΔT_{max}.

For cure time t_{cycle}, increasing the holding-stage temperature CT_2 or decreasing the second heating rate r_2 will clearly extend the cure time, as shown in Fig. 8. The benefit of using higher CT_2 is that we could satisfy the minimum DoC using a shorter holding-stage time t_2. However, using higher CT_2 means that the total time in the second heating-stage will also increase. Therefore, the CT_2 has opposite effect on the cure time between the second heating-stage and second holding-stage. As shown in Fig. 9(a), a minimum cure

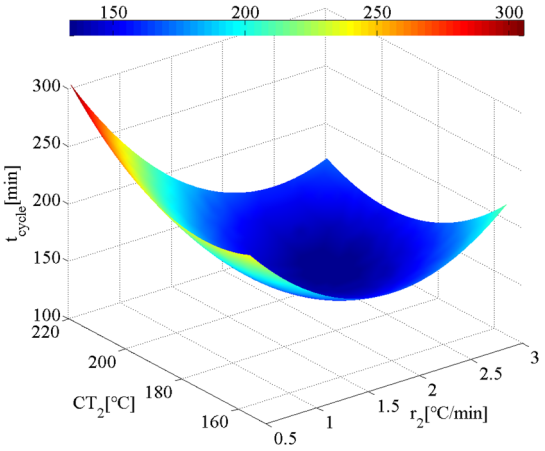

(a) t_{cycle} vs r_2 and CT_2

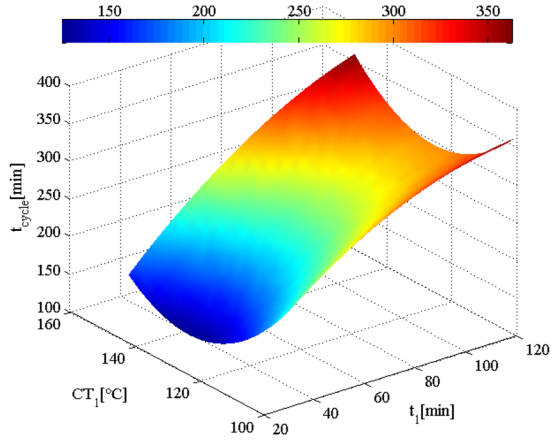

(b) t_{cycle} vs t_1 and CT_1

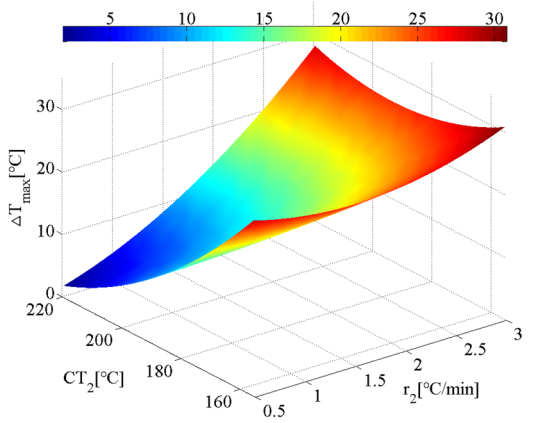

(c) ΔT_{max} vs r_2 and CT_2

Fig. 9 Optimization objectives as a function of input variables

time is reached for the combination between a second holding-stage temperature CT_2 in the 180–210 ℃ range and a second heating rate r_2 in the 1.2–2.2 ℃/min range. Thus, there is a design space to balance the relationship between the holding-stage temperature CT_2 and heating rate r_2. The first holding-stage temperature CT_1 and holding-stage time t_1 also have a reverse effect on the cure time t_{cycle}, and both the relationship is non-linear due to the multi-physical coupling characteristic of cure process, as shown in Fig. 9(b). On the one hand, increasing the first holding-stage temperature CT_1 will accelerate the resin curing reaction at the first holding-stage, thus the resin could fully cure using less time in the rest cure process. On the other hand, when other parameters of the cure profile are unaltered, higher holding-stage temperature CT_1 will increase the cure time at the first heating-stage, which leads to total cure time increasing. However, the cure time at the second heating-stage can be decreased. Taken together, the first holding-stage temperature CT_1 has a reverse effect on the t_{cycle}. Increasing the first holding-stage time t_1 will also increase the total cure time, as shown in Fig. 8. However, the temperature CT_1 and dwelling time t_1 at the first holding-stage has a combined effect on the curing time, as shown in Fig. 9(b). The optimal range for the holding-stage temperature CT_1 is in the range of 110–140 ℃. Therefore, we could use a higher second holding-stage temperature CT_2 to reduce the maximum temperature gradient ΔT_{max}, as shown in Fig. 9(c), and the dwelling time t_2 at the second holding-stage could be also shortened. Meanwhile, we use the intermediate value of the second heating rate r_2 to avoid the dramatically increased of cure time.

A cure cycle profile picked from the Pareto fronts in Fig. 7 is used and the temperature and DoC history of middle, top and bottom regions of the laminate using this cure profile are shown in Fig. 10. It can be seen that both the cure time and maximum temperature gradient have been obviously reduced by using optimized cure profile. The maximum temperature gradient occurred after AGP was 9.6 ℃ and the cure time is 163.13 min. Thus,

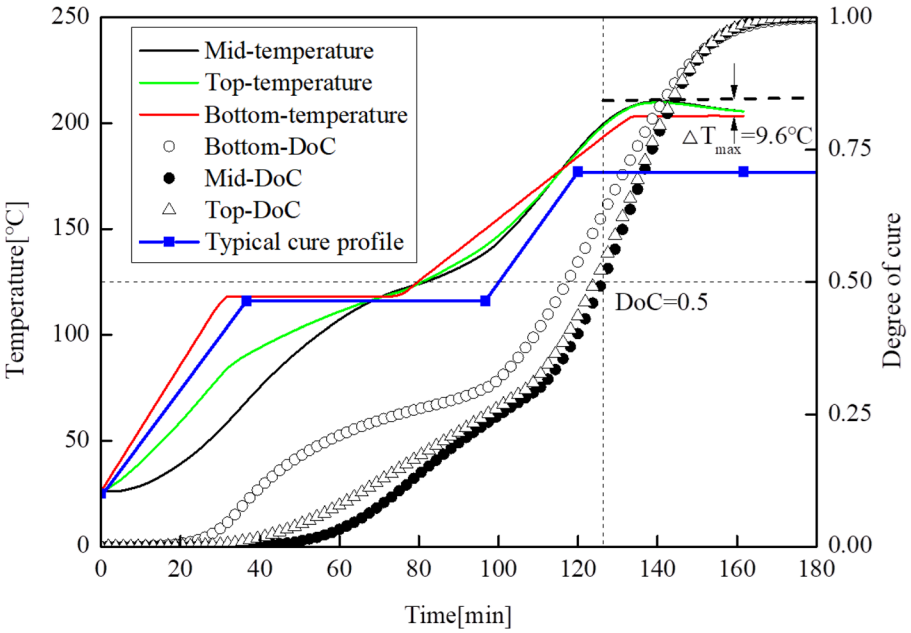

Fig. 10 Temperature and DoC development of the laminate using optimized temperature cycle

the duration of the cure time and the maximum gradient of temperature are about 44.8% and 34% shorter than in the typical cure profile, respectively. The above result also demonstrates that in order to obtain the prescribed minimum value of DoC and decrease maximum temperature gradient in less cure time, the composite part could be cured at higher holding-stage temperature CT_1 and higher holding-stage temperature CT_2. As we can see, the first holding-stage temperature CT_1 at the optimized cure profile is higher than that at the typical cure profile. Increasing the curing temperature CT_1 at the first holding-stage will expedite the curing process. Then, by narrowing the first holding duration t_1 from 60 min to 39.14 min and increasing the first rising rate from 2.22 ℃/min to 2.99 ℃/min, the cure time at the first heating and holding stage could be reduced. By comparison, lower heating rate is applied in the optimized cure profile at the second rising stage to decrease the curing rate to avoid more violent exothermic heat generation. As we can see, the second heating rate r_2 decreases form 2.22 ℃/min to 1.47 ℃/min. However, the second heating rate should not be too small to increase the cure time at this stage, as shown in Fig. 9(a). The second holding-stage temperature CT_2 increased from 176.7 ℃ to 203.43 ℃ in order to decrease the maximum temperature gradient and cure time at the second holding-stage. Consequently, the second holding-stage time t_2 can be decreased from 120 min to 30.05 min to reduce total cure time.

To further demonstrate the necessity of the multi-physics coupling model using in the optimization process, the optimized cure profile with resin flow-compaction process into consideration (case A) are compared to the optimized results without resin flow-compaction (case B), as shown in Fig. 11. In case B, we firstly computed the development of temperature and cure degree using the thermo-chemical model with constant fiber volume fraction in the Eq. (1) and Eq. (2). Then, the temperature and cure degree are used in

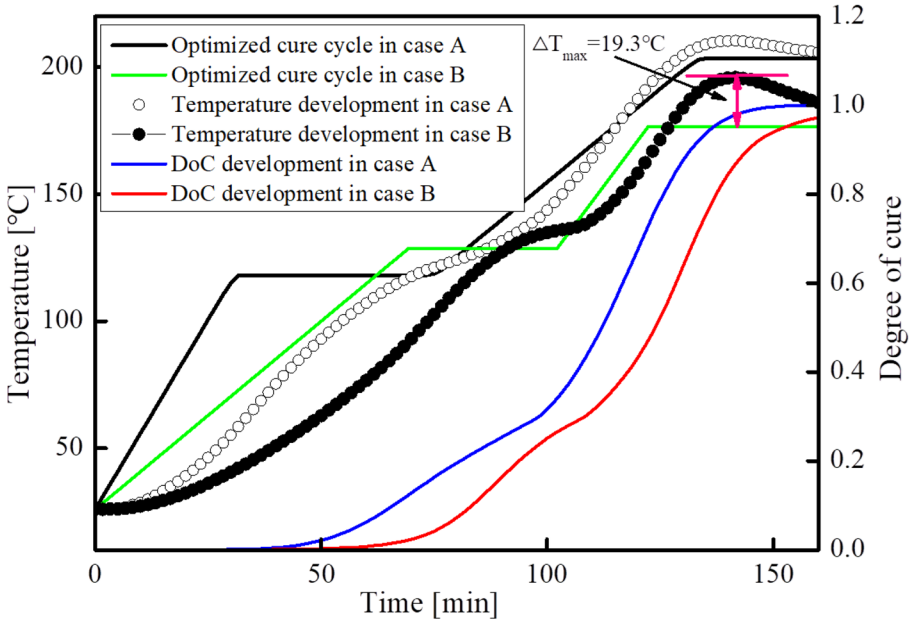

Fig. 11 Temperature and DoC development at the middle region of the laminate using different optimization method

the viscosity model and resin flow-compaction model to calculate the resin viscosity, resin pressure and laminate thickness. Therefore, the variation of fiber volume fraction due to the resin flow-compaction process and its effect on material properties and heat transfer process was not accounted for in the cure simulation. Actually the simulation model in case B is a weakly coupled cure-consolidation model, in which the thermo-chemical model and resin flow-compaction model are not fully coupled. In the similar manner, we use the 140 samples in the previous study to derive the surrogate model and the accuracy of the surrogate model is also verified using another 10 new simulation samples. Then we used the established surrogate model to optimize the cure profile. After the optimization process, we use the new optimized curing profile derived from case B to calculate the development of temperature and DoC by the multi-physics FE model. It should be noted that lots of optimal results will be obtained in the Pareto Front results. Under these circumstances, the objective of the optimization is to reduce the cure time as much as possible under the condition of reducing the maximum temperature gradient by 34%. As we can see, there is a notable difference in the optimized cure profile between the model with- and without- resin flow-compaction process into account. After the cure cycle is over, both the minimum DoC in case A and B is satisfied. However, the maximum temperature gradient T_{max} for the optimized cure cycle with- and without multi-physical characteristics is 9.6 ℃ and 19.3 ℃, respectively. Although the minimum DoC is ensured and the total cure time is shortened in case B, the maximum temperature gradient is higher than the temperature gradient calculated in case A. The development of DoC is also different for the two different cases. The difference is less significant for thin laminate because the maximum temperature gradient during cure process is not obvious. However, it is very important to consider the resin flow-compaction behavior of the laminate in the optimization process for the thick composite component which has been generally ignored in the previous studies.

5 Conclusions

A method combining the multi-physics coupling model with the NSGA-II optimization technique for determining the cure cycle profile has been proposed for PMCs. By taking the effect of heat transfer, cure kinetics, resin flow-compaction process into consideration, a multi-physics coupling finite element model has been developed to predict the information of temperature and DoC. Then, RSM model and NSGA-II algorithm is applied to determine the optimal cure profile. The optimization objectives include minimizing maximum temperature gradient and cure time. Following conclusions can be derived from the above investigation.

1 The relationships between the cure process parameters and the responses of maximum temperature gradient and cure time are established by RSM models. The error tests have shown that the established surrogate models can predict the cure process with small prediction errors.
2 The optimized results show that the cure time and maximum temperature gradient can be decrease at the specified minimum degree of cure (DoC = 0.96) using the optimized cure profile. Compared with the typical cure cycle, the duration of the cure time and the maximum gradient of temperature have been decreased about 44.8% and 34% using optimal cure profile for a 35.75-mm thick laminate, respectively. The findings of the

current study demonstrate that optimized cure cycle can be applied to deliver faster processing with high manufacturing quality.

3 It is also shown that the multi-physics coupling characteristic should be considered in the optimization process for thick composite component.

4 The proposed model can provide a reliable guidance for cure profile design of thick laminate and capabilities for on-line monitoring and control of the cure process.

Acknowledgements The authors would like to acknowledge the financial supports by National Nature Science Foundation of China (51575442, 51805430, 51805429) and Shaanxi Natural Science Foundation (2019JQ-183).

References

1. Wang, H., Chen, L., Ye, F., Wang, J.: A multi-hierarchical successive optimization method for reduction of spring-back in autoclave forming. Compos. Struct. **188**, 143–158 (2018)
2. Struzziero, G., Teuwen, J.J.E.: Effect of convection coefficient and thickness on optimal cure cycles for the manufacturing of wind turbine components using VARTM. Compos. A: Appl. Sci. Manuf. **123**, 25–36 (2017)
3. Wang, L., Xu, P., Peng, X., Zhao, K., Wei, R.: Characterization of inter-ply slipping behaviors in hot diaphragm preforming: experiments and modelling. Compos. A: Appl. Sci. Manuf. **121**, 28–35 (2017)
4. Garschke, C., Weimer, C., Parlevliet, P.P., Fox, B.L.: Out-of-autoclave cure cycle study of a resin film infusion process using in situ process monitoring. Compos. A: Appl. Sci. Manuf. **43**, 935–944 (2017)
5. Ruiz, E., Trochu, F.: Multi-criteria thermal optimization in liquid composite molding to reduce processing stresses and cycle time. Compos. A: Appl. Sci. Manuf. **37**, 913–924 (2006)
6. Sorrentino, L., Esposito, L., Bellini, C.: A new methodology to evaluate the influence of curing overheating on the mechanical properties of thick FRP laminates. Compos. Part B **109**, 187–196 (2016)
7. He, H.W., Li, K.X.: Effect of processing parameters on the interlaminar shear strength of carbon fiber/epoxy composites. J. Macromol. Sci. B. **53**, 1050–1058 (2014)
8. Hernández, S., Sket, F., González, C., Llorca, J.: Optimization of curing cycle in carbon fiber-reinforced laminates Void distribution and mechanical properties. Compos Sci Technol **85**, 85–95 (2013)
9. XW, Zhang., H, Liu., LP, Tu.: A modified particle swarm optimization for multimodal multi-objective optimization. Eng. Appl. Artif. Intel. **95**, 103905 (2020)8
10. Wang, L., Li, H., Bu, X.: Multi-objective optimization of Binary Flashing Cycle (BFC) driven by geothermal energy. Appl. Therm. Eng. **166**, 114693 (2020)
11. Li, K., Yan, S., Zhong, Y., Pan, W., Zhao, G.: Multi-Objective Optimization of the Fiber-reinforced Composite Injection Molding Process using Taguchi method, RSM, and NSGA-II. Simul. Model. Pract. Th. **91**, 69–82 (2019)
12. Faran, R., Ibrahim, D., Kamiel, G.: A multi-objective optimization of the integrated copper-chlorine cycle for hydrogen production. Comput. Chem. Eng. Th. **140**, 106889 (2020)
13. Optimal curing for thermoset matrix composites: Li, M., C.L. Tucker III. Thermochemical and consolidation considerations. Polym Compos. **23**, 118–131 (2002)
14. Neeraj, R., Ranga, P.: Optimal cure cycles for the fabrication of thermosetting-matrix composites. Polym Compos. **18**, 566–581 (1997)
15. Mawardi, A., Pitchumani, R.: Optimal temperature and current cycles for curing of composites using embedded resistive heating elements. J Heat Trans-T Asme. **125**, 127–136 (2003)
16. Dolkun, D., Zhu, W., Xu, Q., Ke, Y.: Optimization of cure profile for thick composite parts based on finite element analysis and genetic algorithm. J. Compos. Mater. **52**, 3885–3894 (2018)
17. Struzziero, G., Skordos, A.A.: Multi-objective optimisation of the cure of thick components. Compos. A: Appl. Sci. Manuf. **93**, 126–136 (2017)
18. Carlone, P., Aleksendrić, D., Ćirović, V., Palazzo, G.S.: Meta-modeling of the curing process of thermoset matrix composites by means of a FEM–ANN approach. Compos. Part B **67**, 441–448 (2014)
19. Vafayan, M., Ghoreishy, M.H.R., Abedini, H., Beheshty, M.H.: Development of an optimized thermal cure cycle for a complex-shape composite part using a coupled finite element/genetic algorithm technique. Iran. Polym. J. **24**, 459–469 (2015)

20. Shah, P.H., Halls, V.A., Zheng, J.Q., Batra, R.C.: Optimal cure cycle parameters for minimizing residual stresses in fiber-reinforced polymer composite laminates. J. Compos. Mater. **52**, 773–779 (2017)
21. Aleksendrić, D., Carlone, P., Ćirović, V.: Optimization of the temperature-time curve for the curing process of thermoset matrix composites. Appl. Compos. Mater. **23**, 1047–1063 (2016)
22. Tifkitsis, K.I., Mesogitis, T.S., Struzziero, G., Skordos, A.A.: Stochastic multi-objective optimisation of the cure process of thick laminates. Compos. A: Appl. Sci. Manuf. **112**, 383–394 (2018)
23. GutowskI, T.G., Cai, Z., Bauer, S., Boucher, D.: Consolidation experiments for laminate composites. J. Compos. Mater **21**, 650–669 (1987)
24. Young, W.B.: Compacting pressure and cure cycle for processing of thick composite laminates. Compos. Sci. Technol. **54**, 299–306 (1995a)
25. Young, W.B.: Resin flow analysis in the consolidation of multi-directional laminated composites. Polym Compos. **16**, 250–257 (1995b)
26. Li, Y., Li, M., Gu, Y., Zhang, Z.: Numerical and experimental study of the bleeder flow in autoclave process. Appl. Compos. Mater. **18**, 327–336 (2011)
27. Ganapathi, A.S., Joshi, S.C., Chen, Z.: Simulation of bleeder flow and curing of thick composites with pressure and temperature dependent properties. Simul. Model. Pract. Th. **32**, 64–82 (2013)
28. Bogetti, T.A., Gillespie, J.W.J.: Two-dimensional cure simulation of thick thermosetting composites. J. Compos. Mater. **25**, 239–273 (1991)
29. White, S.R., Hahn, H.T.: Process modeling of composite materials residual stress development during cure Part II Experimental validation. J Compos Mater **26**, 2423–2453 (1992)
30. Johnston, A.A.: An integrated model of the development of process-induced deformation in autoclave processing of composite structures (1997)
31. Shin, D.D., Hahn, H.T.: Compaction of thick composites: simulation and experiment. Polym. Compos. **25**, 49–59 (2004)
32. Springer, G.S., Tsai, S.W.: Thermal conductivities of unidirectional materials. J. Compos. Mater. **1**, 166–173 (1967)
33. Rolfes, R., Hammerschmidt, U.: Transverse thermal conductivity of CFRP laminates: A numerical and experimental validation of approximation formulae. Compos. Sci. Technol. **54**, 45–54 (1995)
34. Lee, W.I., Loos, A.C., Springer, G.S.: Heat of reaction, degree of cure, and viscosity of hercules 3501–6 resin. J. Compos. Mater. **16**, 510–520 (1982)
35. Dave, R., Kardos, J.L., Duduković, M.P.: A model for resin flow during composite processing: Part 1—general mathematical development. Polym. Compos. **8**, 29–38 (1987)
36. Dave, R.: A unified approach to modeling resin flow during composite processing. J. Compos. Mater. **24**, 22–41 (1990)
37. Young, W.B.: Compacting pressure and cure cycle for processing of thick composite laminates. Compos. Sci Technol. **54**, 299–306 (1995c)
38. Antonucci, V., Giordano, M., Inserraimparato, S., Nicolais, L.: Analysis of heat transfer in autoclave technology. Polym Compos. **22**, 613–620 (2010)
39. Matsuzaki, R., Yokoyama, R., Kobara, T., Tachikawa, T.: Multi-objective curing optimization of carbon fiber composite materials using data assimilation and localized heating. Compos. A: Appl. Sci. Manuf. **119**, 91–72 (2019)
40. Esposito, L., Sorrentino, L., Penta, F., Bellini, C.: Effect of curing overheating on interlaminar shear strength and its modelling in thick FRP laminates. Int. J. Adv. Manuf. Tech. **87**, 2213–2220 (2016)
41. Yeong, K.K., Scott, R.W.: Stress relaxation behavior of 35016 epoxy resin during cure. Polym Engng Sci **36**, 2852–2862 (1996)
42. Yan, L., Qu, Y., Guan, G.: Automatic design optimization of SWATH applying CFD and RSM model. Ocean. Eng. **172**, 146–154 (2019a)
43. Yan, L., Qu, Y., Guan, G.: Scantling optimization of FPSO internal turret area structure using RBF model and evolutionary strategy. Ocean. Eng. **191**, 106562 (2019b)